Proton-^{3}He elastic scattering at low energies and the "A_y Puzzle"

M. Viviani[1,a], L. Girlanda[2], A. Kievsky[1], L. E. Marcucci[2,1], and S. Rosati[2,1]

[1] INFN, Sezione di Pisa, Largo Pontecorvo, 3, 56127 Pisa (Italy)
[2] Phys. Dept., University of Pisa, Largo Pontecorvo, 3, 56127 Pisa (Italy)

Abstract. The Kohn variational principle and the hyperspherical harmonic technique are applied to study $p - {}^3$He elastic scattering at low energies. Preliminary results obtained using several interaction models are reported. The calculations are compared to a recent phase shift analysis performed at the Triangle University Nuclear Laboratory and to the available experimental data. Using a three-nucleon interaction derived from chiral perturbation theory at N^{2}LO, we have found a noticeable reduction of the discrepancy observed for the A_y observable.

1 Introduction

The four nucleon system has been object of intense studies in recent years. In first place, this system is particularly interesting as a "theoretical laboratory" to test the accuracy of our present knowledge of the nucleon–nucleon (NN) and three nucleon (3N) interactions. In particular, the effect of (i) the NN P-wave and of (ii) the 3N force are believed to be larger than in the $A = 2$ or 3 systems. Moreover, it is the simplest system where the 3N interaction in channels of total isospin $T = 3/2$ can be studied. In second place, there is a number of reactions involving four nucleons which are of extreme importance for astrophysics, energy production, and studies of fundamental symmetries. As an example, reactions like $d + d \to {}^4\mathrm{He} + \gamma$ or $p + {}^3\mathrm{He} \to {}^4\mathrm{He} + \nu_\mathrm{e} + \mathrm{e}^+$ (the *hep* process) play important roles in solar models and in the theory of big-bang nucleosynthesis.

Nowadays, the four-nucleon bound state problem can be numerically solved with good accuracy. For example, in Ref. [1] the binding energies and other properties of the α-particle were studied using the AV8′ [2] NN interaction; several different techniques produced results in very close agreement with each other (at the level of less than 1%). More recently, the same agreement has also been obtained considering different realistic NN+3N force models [3,4,5,6].

In recent years, there has also been a rapid advance in solving the four nucleon scattering problem with realistic Hamiltonians. Accurate calculations of four-body scattering observables have been achieved in the framework of the Faddeev-Yakubovsky (FY) equations [7,8,9], solved in momentum space, where the long-range Coulomb interaction is treated using the screening-renormalization method [10,11]. Also solutions of the FY equations in configuration space [12,13,14] and several calculations using the resonating group model [15,16,17,18] were reported. Calculations of scattering observables using the Green Function Monte Carlo method are also underway [19].

In this contribution, the four-body scattering problem is solved using the Kohn variational method and expanding the internal part of the wave function in terms of the hyperspherical harmonic (HH) functions (for a review, see Ref. [20]). Previous applications of this method [21,22,13] were limited to consider only local potentials, as the Argonne v_{18} (AV18) [23] NN potential. Recently, the HH method has been extended to treat also non-local potentials, given either in coordinate- or momentum-space [24,25]. A first application of the HH method to compute $n - {}^3$H elastic observables with non-local potentials was reported in Ref. [26]. Here, we report the first results obtained for $p - {}^3$He.

The potentials used in this paper are the I-N3LO model by Entem and Machleidt [27], with cutoff $\Lambda = 500$ MeV, and the AV18. The I-N3LO potential has been derived using an effective field theory approach and the chiral perturbation theory up to next-to-next-to-next-to-leading order. We have also performed calculations by adding to the I-N3LO potential a 3N interaction, derived at next-to-next-to leading order in Refs. [28,29] (I-N3LO/N-N2LO interaction model). The two free parameters in this N-N2LO 3N potential have been chosen from the combination that reproduces the $A = 3, 4$ binding energies [29]. The development of a 3N interaction including N3LO contribution is still under progress [30]. Finally, we have also considered the Urbana IX (UIX) 3N potential [31], which has been used together with the AV18 potential (AV18/UIX interaction model).

The four-body studies performed so far have evidentiated several discrepancies between the theoretical predictions and experimental data. Let us consider first $n - {}^3$H elastic scattering. Calculations based on NN interaction models only disagree [21,12,32,16,13,7] rather sizably with the measured total cross section [33], both at zero energy and in the "peak" region ($E_n \approx 3.5$ MeV). Such an

[a] e-mail: michele.viviani@pi.infn.it

observable is found to be very sensitive to the NN interaction model [7]. At low energy, the discrepancy is removed by including a 3N force fixed to reproduce the triton binding energy [21,12,16], but it remains in the peak region. Interestingly, this disagreement is noticeably reduced using the I-N3LO/N-N2LO interaction model [26]. A similar situation occurs in the differential cross section, but definitive conclusions in this case are difficult to extract since the experimental errors are rather large.

In this respect, the $p-{}^3$He elastic scattering is more interesting since there exist several accurate measurements of both the unpolarized cross section [34,35,36] and of the proton analyzing power A_y [37,22,36]. The calculations performed so far (with a variety of NN interactions, and with the AV18/UIX model) have shown a glaring discrepancy between theory and experiment for A_y [32,22,16,36,7]. This discrepancy is very similar to the well known "A_y Puzzle" in $N-d$ scattering. This is a fairly old problem, already reported about 20 years ago [38,39] in the case of $n-d$ and later confirmed also in the $p-d$ case [40]. The inclusion of standard models of the 3N force has little effect on these observables. To solve this puzzle, speculations about the deficiency of the NN potentials in ${}^3P_j$ waves (where the spectroscopic notation ${}^{2S+1}L_J$ has been adopted) have been advanced. The situation of other $p-{}^3$He observables (the ^{3}He analyzing power A_{0y} and some spin correlation observables as A_{yy}, A_{xx}, etc.) is less clear due to the lack (until recently) of equally accurate measurements.

However, recently [41,42] at the Triangle University National Lab. (TUNL) there has been a new set of accurate measurements (at $E_p = 1.60$, 2.25, 4 and 5.54 MeV) of various spin correlation coefficients, which has allowed a phase-shift analysis (PSA). The aim of this paper is to compare the results of the theoretical calculations to these new data. Moreover, we want to study the effect of including the N-N2LO 3N force in A_y.

This paper is organized as follows. In Section 2, a brief description of the method is reported. In Section 3, a comparison between HH and FY calculations is shown. We have performed this comparison for $n-{}^3$H scattering using the I-N3LO potential for incident neutron energy $E_n = 3.5$ MeV. In Section 4, the theoretical calculations are compared with the available experimental data. The conclusions will be given in Section 5.

2 The HH Technique for Scattering States

In the following, we consider a $p-{}^3$He scattering state with total angular momentum quantum number JJ_z, and parity π (the dependence on the wave function and other quantities on $JJ_z\pi$ will be understood in the following). The wave function Ψ^{LS}_{1+3} describing the two particles with incoming relative orbital angular momentum L and channel spin S ($S = 0, 1$) can be written as

$$\Psi^{LS}_{1+3} = \Psi^{LS}_C + \Psi^{LS}_A \,, \tag{1}$$

where the part Ψ^{LS}_C vanishes in the limit of large intercluster separations, and hence describes the system in the region where the particles are close to each other and their mutual interactions are strong. On the other hand, Ψ^{LS}_A describes the relative motion of the two clusters in the asymptotic regions, where the $p-{}^3$He interaction is negligible (except for the long-range Coulomb interaction). In the asymptotic region the wave functions Ψ^{LS}_{1+3} reduces to Ψ^{LS}_A, which must therefore be the appropriate asymptotic solution of the Schrödinger equation. Ψ^{LS}_A can be decomposed as a linear combination of the following functions

$$\begin{aligned}\Omega^{\pm}_{LS} &= D_{3+1}\sum_{l=1}^{4}\Big[Y_L(\hat{\mathbf{y}}_l)\otimes[\phi_3(ijk)\otimes s_l]_S\Big]_{JJ_z} \\ &\times\left(f_L(y_l)\frac{G_L(\eta,qy_l)}{qy_l}\pm \mathrm{i}\frac{F_L(\eta,qy_l)}{qy_l}\right), \end{aligned}\tag{2}$$

where y_l is the distance between the proton (particle l) and ^{3}He (particles ijk), q is the magnitude of the relative momentum between the two clusters, s_l the spin state of particle l, and ϕ_3 is the ^{3}He wave function. The total kinetic energy $T_{c.m.}$ in the center of mass (c.m.) system and the proton kinetic energy E_p in the laboratory system are

$$T_{c.m.} = \frac{q^2}{2\mu}\,, \qquad E_p = \frac{4}{3}T_{c.m.}\,, \tag{3}$$

where $\mu = (3/4)M_N$ is the reduced mass of the system (M_N is the nucleon mass). Moreover, F_L and G_L are the regular and irregular Coulomb function, respectively, with $\eta = 2\mu e^2/q$, and D_{3+1} is a normalizing factor defined to be

$$D_{3+1} = \sqrt{\frac{1}{4}}\sqrt{\frac{2\mu q}{\kappa_{3+1}}}\,, \quad \kappa_{3+1} = \sqrt{\frac{3}{2}}\,. \tag{4}$$

The function $f_L(y) = [1-\exp(-\beta y)]^{2L+1}$ in Eq. (2) has been introduced to regularize G_L at small y, and $f_L(y)\to 1$ as y is large, thus not affecting the asymptotic behavior of Ψ^{LS}_{1+3}. Note that for large values of qy_l,

$$\begin{aligned} &f_R(y_l)G_L(\eta,qy_l)\pm \mathrm{i}F_L(\eta,qy_l)\to \\ &\exp\Big[\pm\mathrm{i}\Big(qy_l - L\pi/2 - \eta\ln(2qy_l)+\sigma_L\Big)\Big], \end{aligned}\tag{5}$$

where σ_L is the Coulomb phase shift. Therefore, Ω^{+}_{LS} (Ω^{-}_{LS}) describe the asymptotic outgoing (ingoing) $p-{}^3$He relative motion. Finally,

$$\Psi^{LS}_A = \sum_{L'S'}\Big[\delta_{LL'}\delta_{SS'}\Omega^{-}_{LS} - \mathcal{S}_{LS,L'S'}(q)\Omega^{+}_{L'S'}\Big], \tag{6}$$

where the parameters $\mathcal{S}_{LS,L'S'}(q)$ are the S-matrix elements which determine phase-shifts and (for coupled channels) mixing parameters at the energy $T_{c.m.}$. Of course, the sum over L' and S' is over all values compatible with the given J and parity π. In particular, the sum over L' is limited to include either even or odd values such that $(-1)^{L'} = \pi$.

The "core"wave function Ψ^{LS}_C has been here expanded using the HH basis. For four equal mass particles, a suitable choice of the Jacobi vectors is

$$\boldsymbol{x}_{1p} = \sqrt{\frac{3}{2}}\left(\mathbf{r}_l - \frac{\mathbf{r}_i+\mathbf{r}_j+\mathbf{r}_k}{3}\right),$$

$$\boldsymbol{x}_{2p} = \sqrt{\frac{4}{3}}\left(\mathbf{r}_k - \frac{\mathbf{r}_i + \mathbf{r}_j}{2}\right), \qquad (7)$$
$$\boldsymbol{x}_{3p} = \mathbf{r}_j - \mathbf{r}_i ,$$

where p specifies a given permutation corresponding to the order i, j, k and l of the particles. By definition, the permutation $p = 1$ is chosen to correspond to the order 1, 2, 3 and 4.

For a given choice of the Jacobi vectors, the hyperspherical coordinates are given by the so-called hyperradius ρ, defined by

$$\rho = \sqrt{x_{1p}^2 + x_{2p}^2 + x_{3p}^2}, \quad \text{(independent of } p), \qquad (8)$$

and by a set of angular variables which in the Zernike and Brinkman [43,44] representation are (i) the polar angles $\hat{x}_{ip} \equiv (\theta_{ip}, \phi_{ip})$ of each Jacobi vector, and (ii) the two additional "hyperspherical" angles φ_{2p} and φ_{3p} defined as

$$\cos\phi_{2p} = \frac{x_{2p}}{\sqrt{x_{1p}^2 + x_{2p}^2}}, \quad \cos\phi_{3p} = \frac{x_{3p}}{\sqrt{x_{1p}^2 + x_{2p}^2 + x_{3p}^2}}, \qquad (9)$$

where x_{jp} is the modulus of the Jacobi vector $\boldsymbol{x}_j$. The set of angular variables $\hat{x}_{1p}, \hat{x}_{2p}, \hat{x}_{3p}, \phi_{2p}$, and ϕ_{3p} is denoted hereafter as Ω_p. The expression of a generic HH function is

$$\begin{aligned}
&\mathcal{H}^{K,\Lambda,M}_{\ell_1,\ell_2,\ell_3,L_2,n_2,n_3}(\Omega_p) = \\
&\mathcal{N}^{\ell_1,\ell_2,\ell_3}_{n_2,n_3}\left[\left(Y_{\ell_1}(\hat{x}_{1p})Y_{\ell_2}(\hat{x}_{2p})\right)_{L_2} Y_{\ell_3}(\hat{x}_{3p})\right]_{\Lambda M} \\
&\times \sin^{\ell_1}\phi_{2p}\cos^{\ell_2}\phi_{2p}\sin^{\ell_1+\ell_2+2n_2}\phi_{3p}\cos^{\ell_3}\phi_{3p} \\
&\times P_{n_2}^{\ell_1+\frac{1}{2},\ell_2+\frac{1}{2}}(\cos 2\phi_{2p}) P_{n_3}^{\ell_1+\ell_2+2n_2+2,\ell_3+\frac{1}{2}}(\cos 2\phi_{3p}) , \qquad (10)
\end{aligned}$$

where $P_n^{a,b}$ are Jacobi polynomials and the coefficients $\mathcal{N}^{\ell_1,\ell_2,\ell_3}_{n_2,n_3}$ normalization factors. The quantity $K = \ell_1 + \ell_2 + \ell_3 + 2(n_2 + n_3)$ is the so-called grand angular quantum number. The HH functions are the eigenfunctions of the hyperangular part of the kinetic energy operator. Another important property of the HH functions is that $\rho^K \mathcal{H}^{K,\Lambda,M}_{\ell_1,\ell_2,\ell_3,L_2,n_2,n_3}(\Omega_p)$ are homogeneous polynomials of the particle coordinates of degree K.

A set of antisymmetrical hyperangular–spin–isospin states of grand angular quantum number K, total orbital angular momentum Λ, total spin Σ, and total isospin T (for the given values of total angular momentum J and parity π) can be constructed as follows:

$$\Psi^{K\Lambda\Sigma T}_{\mu} = \sum_{p=1}^{12} \Phi^{K\Lambda\Sigma T}_{\mu}(i,j,k,l) , \qquad (11)$$

where the sum is over the 12 even permutations $p \equiv i, j, k, l$, and

$$\begin{aligned}
&\Phi^{K\Lambda\Sigma T}_{\mu}(i,j;k;l) = \\
&\left\{\mathcal{H}^{K,\Lambda,M}_{\ell_1,\ell_2,\ell_3,L_2,n_2,n_3}(\Omega_p)\left[\left[\left(s_i s_j\right)_{S_a} s_k\right]_{S_b} s_l\right]_{\Sigma}\right\}_{JJ_z} \\
&\times\left[\left[\left(t_i t_j\right)_{T_a} t_k\right]_{T_b} t_l\right]_{TT_z} . \qquad (12)
\end{aligned}$$

Here, $\mathcal{H}^{K,\Lambda,M}_{\ell_1,\ell_2,\ell_3,L_2,n_2,n_3}(\Omega_p)$ is the HH state defined in Eq. (10), and s_i (t_i) denotes the spin (isospin) function of particle i. The total orbital angular momentum Λ of the HH function is coupled to the total spin Σ to give the total angular momentum JJ_z, whereas $\pi = (-1)^{\ell_1+\ell_2+\ell_3}$. The quantum number T specifies the total isospin of the state. The integer index μ labels the possible choices of hyperangular, spin and isospin quantum numbers, namely

$$\mu \equiv \{\ell_1, \ell_2, \ell_3, L_2, n_2, n_3, S_a, S_b, T_a, T_b\} , \qquad (13)$$

compatibles with the given values of K, Λ, Σ, T, J and π. Another important classification of the states is to group them in "channels": states belonging to the same channel have the same values of angular $\ell_1, \ell_2, \ell_3, L_2, \Lambda$, spin S_a, S_b, Σ, isospin T_a, T_b, T quantum numbers but different values of n_2, n_3.

Each state $\Psi^{K\Lambda\Sigma T}_{\mu}$ entering the expansion of the four nucleon wave function must be antisymmetric under the exchange of any pair of particles. Consequently, it is necessary to consider states such that

$$\Phi^{K\Lambda\Sigma T}_{\mu}(i,j;k;l) = -\Phi^{K\Lambda\Sigma T}_{\mu}(j,i;k;l) , \qquad (14)$$

which is fulfilled when the condition

$$\ell_3 + S_a + T_a = \text{odd} , \qquad (15)$$

is satisfied.

The number $M_{K\Lambda\Sigma T}$ of antisymmetrical functions $\Psi^{K\Lambda\Sigma T}_{\mu}$ having given values of K, Λ, Σ, and T but different combinations of quantum numbers μ (see Eq.(13)) is in general very large. In addition to the degeneracy of the HH basis, the four spins (isospins) can be coupled in different ways to Σ (T). However, many of the states $\Psi^{K\Lambda\Sigma T}_{\mu}$, $\mu = 1, \ldots, M_{K\Lambda\Sigma T}$ are linearly dependent between themselves. In the expansion of Ψ^{LS}_{C} it is necessary to include only the subset of linearly independent states, whose number is fortunately noticeably smaller than the corresponding value of $M_{K\Lambda\Sigma T}$.

The internal part of the wave function can be finally written as

$$\Psi^{LS}_{C} = \sum_{K\Lambda\Sigma T}\sum_{\mu} u^{LS}_{K\Lambda\Sigma T\mu}(\rho)\Psi^{K\Lambda\Sigma T}_{\mu} , \qquad (16)$$

where the sum is restricted only to the linearly independent states. We have found convenient to expand the "hyperradial" functions $u^{LS}_{K\Lambda\Sigma T\mu}(\rho)$ in a complete set of functions, namely

$$u^{LS}_{K\Lambda\Sigma T\mu}(\rho) = \sum_{m=0}^{M-1} c^{LS}_{K\Lambda\Sigma T\mu,m}\, g_m(\rho) , \qquad (17)$$

and we have chosen

$$g_m(\rho) = \sqrt{\gamma^9 \frac{m!}{(m+8)!}}\; L_m^{(8)}(\gamma\rho)\; \mathrm{e}^{-\frac{\gamma}{2}\rho} , \qquad (18)$$

where $L_l^{(8)}(\gamma\rho)$ are Laguerre polynomials [45] and γ is a parameter to be variationally optimized.

The main problem is the computation of the matrix elements of the Hamiltonian. This task is considerably simplified in two steps. First, by using the following transformation

$$\Phi_{\mu}^{K\Lambda\Sigma T}(i,j;k;l) = \sum_{\mu'} a_{\mu,\mu'}^{K\Lambda\Sigma T}(p)\Phi_{\mu'}^{K\Lambda\Sigma T}(1,2;3;4)\,, \quad (19)$$

where the coefficients $a_{\mu,\mu'}^{K\Lambda\Sigma T}(p)$ have been obtained using the techniques described in Ref. [46]. Second, by "projecting" the asymptotic states over a complete set of angular-spin-isospin states, constructed in terms of the Jacobi vectors $\boldsymbol{x}_i$ corresponding to the particle order $1,2,3,4$, as follows:

$$\Omega_{LS}^{\pm} = \sum_{\alpha} F_{\alpha}^{LS\pm}(x_1,x_2,x_3)\mathcal{Y}_{\alpha}(\hat{x}_1,\hat{x}_2,\hat{x}_3)\,, \quad (20)$$

where

$$\mathcal{Y}_{\alpha}(\hat{x}_1,\hat{x}_2,\hat{x}_3) = \left\{\left[\left(Y_{\ell_3}(\hat{x}_3)(s_1s_2)_{S_2}\right)_{j_3}\left(Y_{\ell_2}(\hat{x}_2)s_3\right)_{j_2}\right]_{J_2} \left(Y_{\ell_1}(\hat{x}_1)s_4\right)_{j_1}\right\}_{JJ_z}\left[\left[(t_1t_2)_{T_2}t_3\right]_{T_3}t_4\right]_{TT_z} \quad (21)$$

and $\alpha = \{\ell_1,\ell_2,\ell_3,j_1,j_2,j_3,J_2,S_2,T_2,T_3,T\}$. Note that due to the antisymmetry of the wave function, we must have $\ell_3 + S_2 + T_2 =$ odd. This "partial wave expansion" is performed to include all states α such that $\ell_i \le \ell_{\max}$. The functions $F_{\alpha}^{LS\pm}$ can be obtained very accurately by direct integration

$$F_{\alpha}^{LS\pm}(x_1,x_2,x_3) = \int d\hat{x}_1 d\hat{x}_2 d\hat{x}_3 \left[\mathcal{Y}_{\alpha}(\hat{x}_1,\hat{x}_2,\hat{x}_3)\right]^{\dagger}\Omega_{LS}^{\pm}\,, \quad (22)$$

using Gauss quadrature techniques.

Finally, the wave function using the transformation (19) and the partial wave expansion given above can be rewritten as

$$\Psi_{1+3}^{LS} = \sum_{\alpha}\mathcal{F}_{\alpha}^{LS}(x_1,x_2,x_3)\mathcal{Y}_{\alpha}(\hat{x}_1,\hat{x}_2,\hat{x}_3)\,, \quad (23)$$

where $\mathcal{F}$ is a combination of Jacobi polynomials of the hyperangles, functions $g_m(\rho)$, and functions F_{α} coming from the asymptotic parts. Then, the matrix elements of a two-body potential can be evaluated as following. First of all

$$\langle\Psi_{1+3}^{LS}|\sum_{i<j}V(i,j)|\Psi_{1+3}^{L'S'}\rangle = 6\langle\Psi_{1+3}^{LS}|V(1,2)|\Psi_{1+3}^{L'S'}\rangle\,, \quad (24)$$

due to the asymmetry of the wave function. The matrix element of $V(1,2)$ (note that $\boldsymbol{x}_3 = \mathbf{r}_2 - \mathbf{r}_1$) is easily obtained using the decomposition given in Eq. (23). For example, for a non-local potential

$$\langle\Psi_{1+3}^{LS}|V(1,2)|\Psi_{1+3}^{L'S'}\rangle = \int d^3\boldsymbol{x}_1 d^3\boldsymbol{x}_2 d^3\boldsymbol{x}_3 d^3\boldsymbol{x}_3'\left(\Psi_{1+3}^{LS}(\boldsymbol{x}_1,\boldsymbol{x}_2,\boldsymbol{x}_3)\right)^{\dagger} \times V(\boldsymbol{x}_3,\boldsymbol{x}_3')\Psi_{1+3}^{L'S'}(\boldsymbol{x}_1,\boldsymbol{x}_2,\boldsymbol{x}_3')\,. \quad (25)$$

Table 1. Phase-shift and mixing angle parameters for $n - {}^3$H elastic scattering at incident neutron energy $E_n = 3.5$ MeV calculated using the I-N3LO potential. The values reported in the columns labeled HH have been obtained using the HH expansion and the Kohn variational principle, whereas those reported in the columns labeled FY by solving the FY equations [8].

Phase-shift	HH	FY	Phase-shift	HH	FY
$^1S_0$	−65.66	−65.54	$^3P_0$	20.21	20.31
$^3S_1$	−58.20	−57.99	$^1P_1$	20.90	20.74
$^3D_1$	− 0.92	− 0.91	$^3P_1$	40.98	40.94
ϵ	− 0.67	− 0.72	ϵ	9.57	9.45
$^1D_2$	− 1.45	− 1.59	$^3P_2$	43.58	43.98
$^3D_2$	− 0.82	− 0.84	$^3F_2$	0.05	0.07
ϵ	2.63	2.49	ϵ	1.14	1.17

The calculation of the above integral is performed in two steps. First, the spin-isospin-angular matrix elements

$$\int d\hat{x}_1 d\hat{x}_2 d\hat{x}_3 d\hat{x}_3'\ \mathcal{Y}_{\alpha}(\hat{x}_1,\hat{x}_2,\hat{x}_3)^{\dagger} \times V(\boldsymbol{x}_3,\boldsymbol{x}_3')\ \mathcal{Y}_{\alpha'}(\hat{x}_1,\hat{x}_2,\hat{x}_3') = v_{\ell_3,S_2,\ell_3',S_2'}^{j_3,T_3,T,T_3',T'}(x_3,x_3')\delta_{j_3,j_3'}\delta_{j_2,j_2'}\delta_{j_1,j_1'}\delta_{\ell_2,\ell_2'}\delta_{\ell_1,\ell_1'}\,, \quad (26)$$

are computed analytically, and, second, the integration over the moduli of the Jacobi vectors,

$$\int_0^{\infty} dx_1 dx_2 dx_3 dx_3'\ x_1^2x_2^2x_3^2x_3'^2\left(\mathcal{F}_{\alpha}^{LS}(x_1,x_2,x_3)\right)^{*} \times v_{\ell_3,S_2,\ell_3',S_2'}^{j_3,T_3,T,T_3',T'}(x_3,x_3')\,\mathcal{F}_{\alpha'}^{L'S'}(x_1,x_2,x_3')\,, \quad (27)$$

can easily obtained by using Gauss quadrature methods, being a 4-dimensional integral. The accuracy of the matrix elements so calculated depends mainly on $\ell_{\max}$, the maximum value of the orbital angular momentum used to truncate the expansion (20). Values $\ell_{\max} = 5$ or 6 have been found appropriate to obtain a sufficient numerical accuracy.

The S-matrix elements $\mathcal{S}_{LS,L'S'}(p)$ and coefficients $c_{K\Lambda\Sigma T\mu,m}^{LS}$ occurring in the expansion of Ψ_C^{LS} are determined by making the functional

$$[\overline{\mathcal{S}}_{LS,L'S'}(q)] = \mathcal{S}_{LS,L'S'}(q) - \frac{1}{2i}\left\langle\Psi_{1+3}^{L'S'}\,|H-E|\,\Psi_{1+3}^{LS}\right\rangle \quad (28)$$

stationary with respect to variations in the $\mathcal{S}_{LS,L'S'}$ and $c_{K\Lambda\Sigma T\mu,m}^{LS}$ (Kohn variational principle). By applying this principle, a linear set of equations for $\mathcal{S}_{LS,L'S'}$ and $c_{K\Lambda\Sigma T\mu,m}^{LS}$ is obtained. The linear system is solved using the Lanczos algorithm.

The main difficulty of the application of the HH technique is the slow convergence of the basis with respect to the grand angular quantum number K. This problem has been overcome by dividing the HH basis in *classes*. More details of this method can be found in Ref. [36].

3 Comparison between HH and FY results

The calculated phase-shift and mixing angle parameters for $n - {}^3$H elastic scattering at $E_n = 3.5$ MeV using the

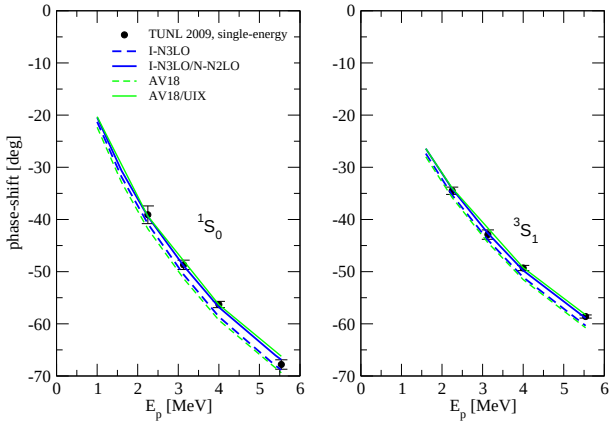

Fig. 1. p – ^{3}He S-wave phase shifts for four potential models. The results of the PSA performed at TUNL have been also reported [42].

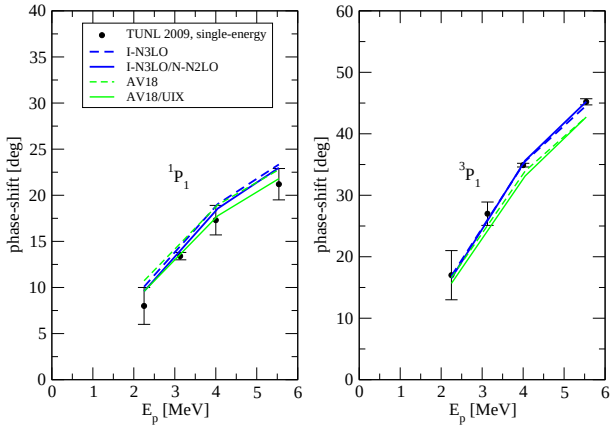

Fig. 2. As in Fig. 1 but for the $^1P_1$ and $^3P_1$ phase shifts.

I-N3LO potential are reported in Table 1. The values reported in the columns labeled HH have been obtained using the HH expansion and the Kohn variational principle, whereas those reported in the columns labeled FY by solving the FY equations [8]. As can be seen, there is a good overall agreement between the results of the two calculations. Similar comparisons for $p-^3$He are currently underway.

4 Results

In this Section, we present preliminary calculations of elastic p – ^{3}He observables. Final results with complete tests of convergence with respect to K and $\ell_{\rm maax}$ will be reported in a forthcoming paper.

In the energy range considered here ($E_p \leq 6$ MeV), the various p – ^{3}He observables are dominated by S-wave and P-wave phase-shifts (D-wave phase shifts give only a marginal contribution, and more peripheral phase shifts are negligible). Let us first concentrate on the comparison of calculated S-wave and P-wave phase shifts with those obtained by the recent PSA [42], shown in Figs. 1–4. The $^1S_0$ and $^3S_1$ phase shifts are reported in Fig. 1. The results obtained including NN interactions only slightly overpredict (in absolute value) the PSA values. Including the 3N force, the calculated phase shifts agree very well with the PSA values (for both AV18/UIX and I-N3LO/N-N2LO models). In fact, the p – ^{3}He interaction in S-wave is repulsive, being dominated by the Pauli repulsion, and the corresponding phase shifts are generally well reproduced by an interaction model giving the correct value of the ^{3}He binding energy (and radius).

In Fig. 2, the comparison is shown for the $J^\pi = 1^-$ phase shifts. The PSA values for the $^1P_1$ phase shift have large error bars and all potential models give results consistent with them. In general, we observe that the inclusion of the 3N interaction reduces such a phase shift. For the $^3P_1$ phase shift, we observe that the theoretical results obtained with AV18 and AV18/UIX models disagree with the PSA values, in particular for $E_p \geq 4$ MeV. Moreover, the inclusion of the UIX 3N force diminishes the phase shift, enlarging the discrepancy. On the contrary, the results obtained with I-N3LO and I-N3LO/N-N2LO are very close to the data. The inclusion of such a 3N force slightly increases the $^3P_1$ phase shift.

A similar behavior can be observed for the $^3P_2$ and $^3P_0$ phase shifts, reported in Fig. 3. The $^3P_2$ phase shift is well reproduced by I-N3LO and I-N3LO/N-N2LO models,

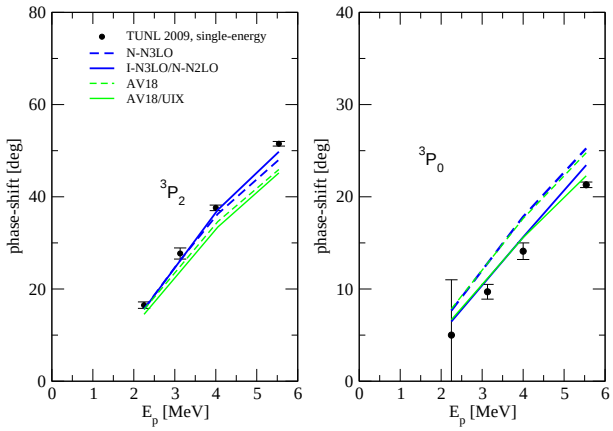

Fig. 3. As in Fig. 1 but for the $^3P_2$ and $^3P_0$ phase shifts.

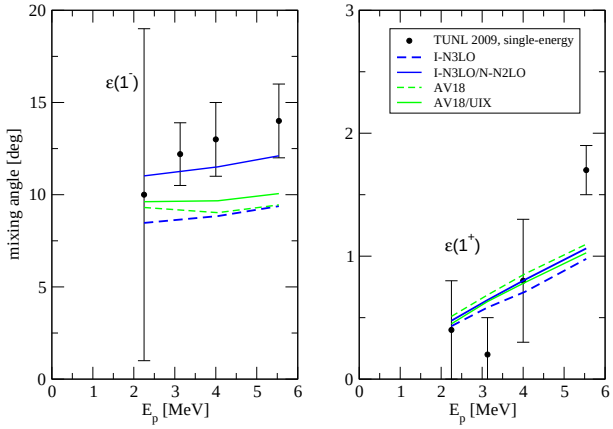

Fig. 4. As in Fig. 1 but for the 1^- and 1^+ mixing parameters.

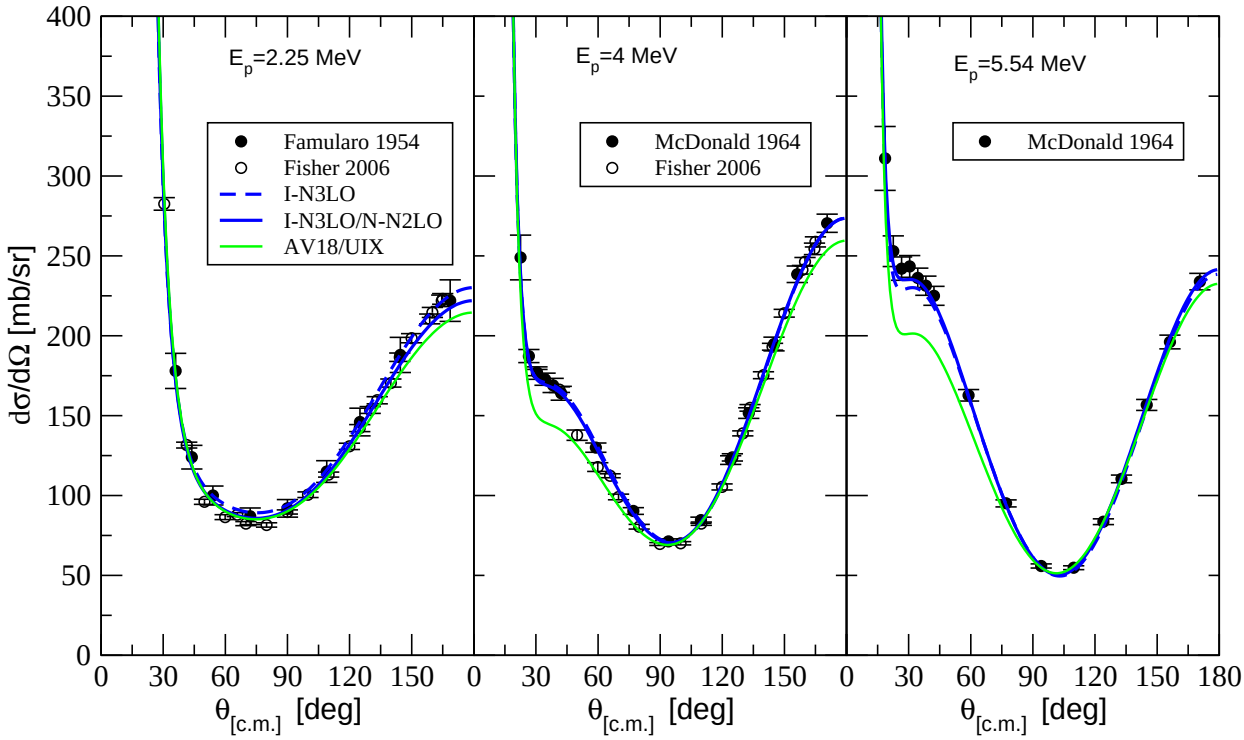

Fig. 5. p – ^{3}He differential cross sections calculated with the I-N3LO (blue dashed line), the I-N3LO/N-N2LO (blue solid line), and the AV18/UIX (thin green solid line) interaction models for three different incident proton energies. The experimental data are from Refs. [34,35,36].

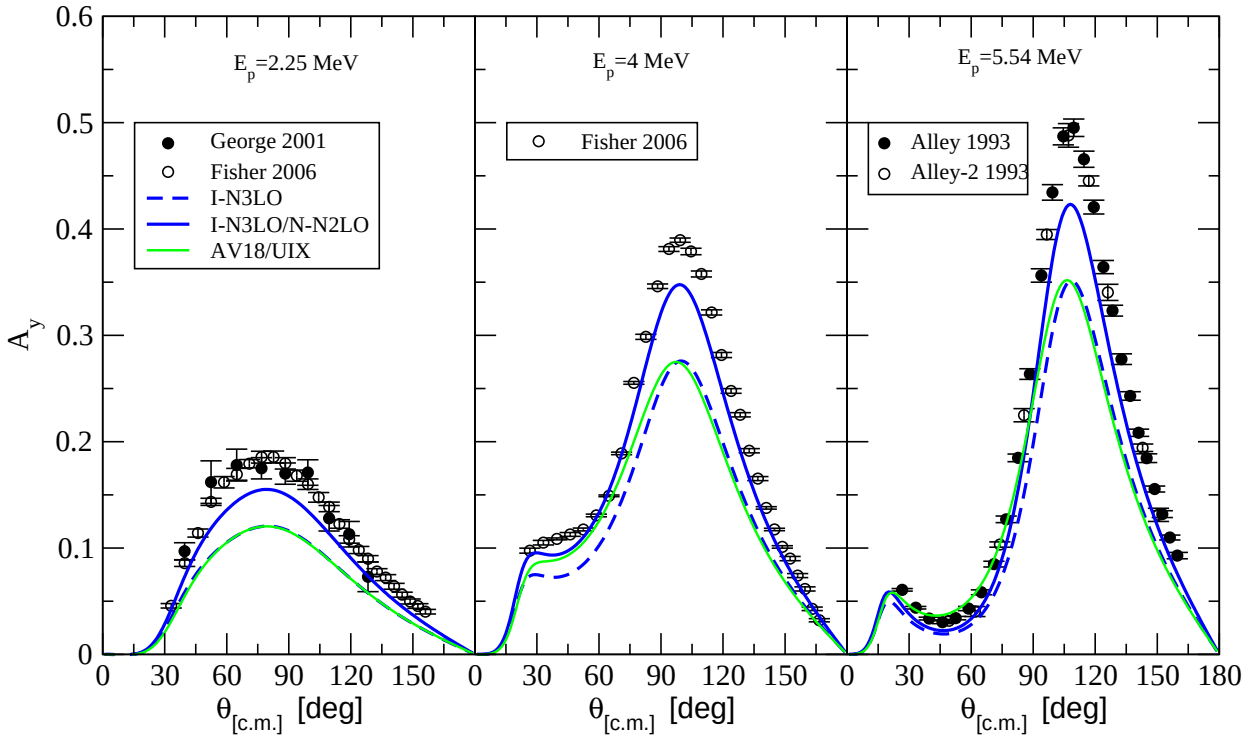

Fig. 6. p – ^{3}He A_y observable calculated with the I-N3LO (blue dashed line), the I-N3LO/N-N2LO (blue solid line), and the AV18/UIX (thin green solid line) interaction models for three different incident proton energies. The experimental data are from Refs. [37,22,36].

while with AV18 and AV18/UIX we observe an underprediction. For the $^3P_0$ phase shift we observe that the models including NN interaction only overpredict the PSA values. With the inclusion of the 3N forces, the results come close to the PSA values. This behavior is not unexpected, as it was already known that this phase shift "scales" with the ^{3}He binding energy [7].

Finally, in Fig. 4 the comparison is performed for the 1^- and 1^+ mixing parameters. For $\varepsilon(1^-)$, the PSA results have quite large errors, however it is significant that only the I-N3LO/N-N2LO values are in the error bar. For $\varepsilon(1^+)$, the results obtained with all the four models are more less consistent with the (largely scattered) PSA values.

In conclusion, with AV18, the S-wave and most of the P-wave phase shifts are at variance with the results of the PSA. Including the UIX 3N force, only the S-wave shifts are adjusted. With I-N3LO, the S-wave phase shifts are overpredicted (in absolute value), but the P-wave phase shifts are much better reproduced. Including the N-N2LO 3N interaction, the S-wave shifts become well reproduced, while the agreement with the P-wave shifts is not spoiled. In this case also the mixing parameters are well reproduced. We observe therefore an overall good agreement between the results obtained with the I-N3LO/N-N2LO model and the PSA values.

Let us now compare the results of the calculations directly with the available experimental data. The potential models considered hereafter are the I-N3LO, I-N3LO/N-N2LO, and AV18/UIX. The calculated $p-{}^3$He differential cross sections a energies $E_p = 2.25$, 4, and 5.54 MeV are reported in Fig. 5 and compared with the experimental data of Refs. [34,35,36]. As can be seen, there is a good agreement between the theoretical calculations and experimental data. In fact, this observable is sensitive to small changes of the phase shifts only in the "interference" region around $\theta = 30$ deg. We note only a slight deviation of the AV18/UIX results from the data in such a region.

More interesting is the situation for the proton vector analyzing power A_y. Here, we observe a larger sensitivity to the employed interaction model. The calculations performed using AV18/UIX largely underpredict the experimental points, a fact already observed before [22,36]. Using I-N3LO, no significative changes are observed. A sizable improvement is found by adopting the I-N3LO/N-N2LO model, as it was expected from the discussion regarding the comparison with the PSA phase shifts. To be more quantitative, let us consider the ratio $A_y^{\rm theor}/A_y^{\rm expt}$ at the peak, reported in Table 2. For the AV18, AV18/UIX, and I-N3LO models, there is approximately a 30% underprediction of the peak height. The underprediction is reduced approximately by a factor 2 for the I-N3LO/N-N2LO model.

Finally, in Figs. 7 and 8, we show two further polarization observables, the ^{3}He analyzing power A_{y0} and the spin correlation coefficient A_{yy}. These observables (and other spin correlation coefficients) are not very sensitive to the interaction model. We observe however, that the I-N3LO/N-N2LO model produces slightly better agreement with data.

Table 2. Ratio $A_y^{\rm theor}/A_y^{\rm expt}$ at the peak for the four potential models and three values of proton energy E_p.

Pot.	2.25 MeV	4 MeV	5.54 MeV
AV18	0.64	0.65	0.67
AV18/UIX	0.66	0.70	0.71
I-N3LO	0.66	0.70	0.71
I-N3LO/N-N2LO	0.87	0.88	0.86

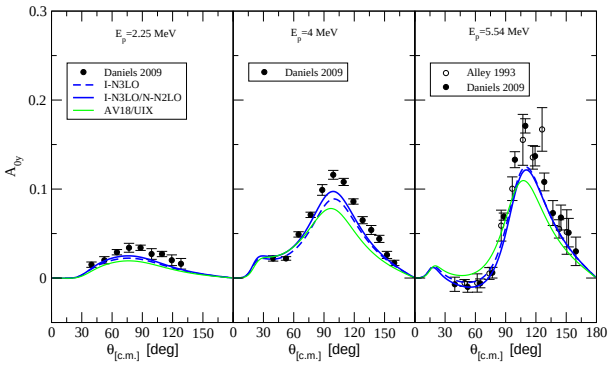

Fig. 7. $p-{}^3$He observable A_{0y} calculated with the I-N3LO (blue dashed line), the I-N3LO/N-N2LO (blue solid line), and the AV18/UIX (thin green solid line) interaction models for three different incident proton energies. The experimental data are from Refs. [37,41].

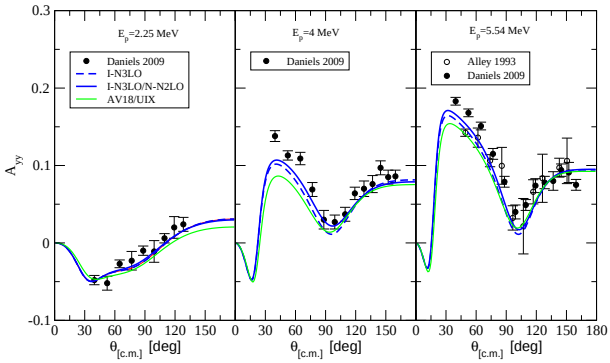

Fig. 8. $p-{}^3$He observable A_{yy} calculated with the I-N3LO (blue dashed line), the I-N3LO/N-N2LO (blue solid line), and the AV18/UIX (thin green solid line) interaction models for three different incident proton energies. The experimental data are from Refs. [37,41].

5 Conclusions

In this paper preliminary results for $p-{}^3$He elastic scattering obtained using the HH function expansion have been reported. We have considered four interaction models. The first two are based on phenomenological NN interactions (AV18 and AV18/UIX). The other two are derived from a chiral effective theory (I-N3LO and I-N3LO/N-N2LO). Both NN interactions (AV18 and I-N3LO) reproduce the NN scattering data with a χ^2 per datum very close to 1. The UIX 3N interaction has been fixed in order to reproduce the trinucleon binding energies, whereas the N-N2LO by fitting simultaneously both $A = 3, 4$ binding energies.

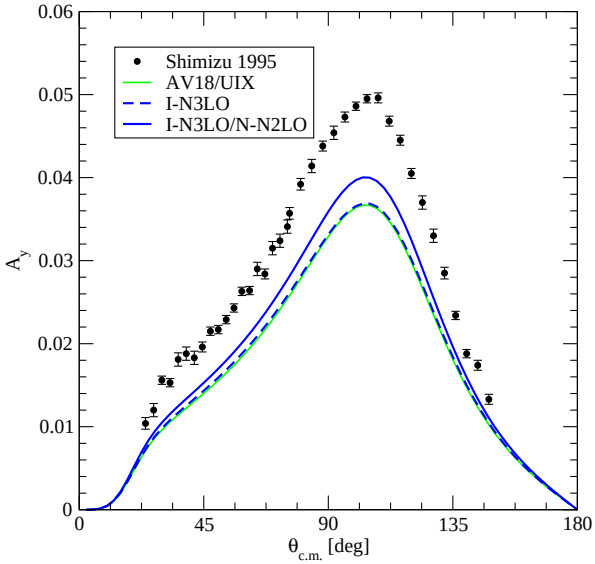

Fig. 9. $p-d$ observable A_y at $E_p = 3$ MeV calculated with the I-N3LO (blue dashed line), I-N3LO/N-N2LO (blue solid line), and AV18/UIX (thin green solid line) interaction models for $E_p = 3$ MeV. The experimental data are from Ref. [47].

We have compared the results obtained with the four interaction models with the available experimental data and a very recent PSA performed at TUNL [42]. We have found that the phase shifts obtained with I-N3LO/N-N2LO are consistent with those derived from the PSA. The direct comparison of the I-N3LO/N-N2LO results with the experimental data has shown that there are still some discrepancies, but the A_y problem is noticeably reduced. In fact, we observe that now the discrepancy is of the order of 15% at the peak, much less than what observed with other interaction models.

In this regard, it is interesting to note that in the $N-d$ case, the use of the I-N3LO/N-N2LO model does not give such a reduction of the $N-d$ "A_y Puzzle", as can be seen for example in Fig. 9. We observe in fact only a small increase of the A_y computed with the I-N3LO/N-N2LO model with respect to that calculated, for example, using the AV18/UIX model. Note that also for $p-d$, the calculated A_y with I-N3LO and AV18/UIX are very similar. In this case the ratio $A_y^{\rm theor}/A_y^{\rm expt}$ at the peak is approximately 0.81 (0.74) for I-N3LO/N-N2LO (AV18/UIX). Investigations to understand this behavior are in progress.

Acknowledgments. We would like to thank T.V. Daniels and T.B. Clegg for providing us with their experimental data prior to publication, and A. Deltuva and A. Fonseca for useful discussions.

References

1. H. Kamada *et al.*, Phys. Rev. C **64**, (2001) 044001
2. B. S. Pudliner *et al.*, Phys. Rev. C **56**, (1997) 1720
3. A. Nogga *et al.*, Phys. Rev. C **67**, (2003) 034004
4. R. Lazauskas and J. Carbonell, Phys. Rev. C **70**, (2004) 044002
5. M. Viviani, A. Kievsky, and S. Rosati, Phys. Rev. C **71**, (2005) 024006
6. R.B. Wiringa *et al.*, Phys. Rev. C **62**, (2000) 014001
7. A. Deltuva and A. C. Fonseca, Phys. Rev. C **75**, (2007) 014005
8. A. Deltuva and A. C. Fonseca, Phys. Rev. Lett. **98**, (2007) 162502
9. A. Deltuva and A. C. Fonseca, Phys. Rev. C **76**, (2007) 021001
10. E. O. Alt, W. Sandhas, and H. Ziegelmann, Phys. Rev. C **17**, (1978) 1981; *ibid.*. **21**, (1980) 1733
11. A. Deltuva, A. C. Fonseca, and P.U. Sauer, Phys. Rev. C **71**, (2005) 054005; *ibid.*, **72**, (2005) 054004
12. F. Cieselski and J. Carbonell, Phys. Rev. C **58**, (1998) 58; F. Cieselski, J. Carbonell, and C. Gignoux, Phys. lett. **B447**, (1999) 199
13. R. Lazauskas *et al.*, Phys. Rev. C **71**, (2005) 034004
14. R. Lazauskas, Phys. Rev. C **79**, (2009) 054007
15. H. M. Hofmann and G. M. Hale, Nucl. Phys. **A613**, (1997) 69
16. B. Pfitzinger, H. M. Hofmann, and G. M. Hale, Phys. Rev. C **64**, (2001) 044003
17. H. M. Hofmann and G. M. Hale, Phys. Rev. C **68**, (2003) 021002; Phys. Rev. C **77**, (2008) 044002
18. S. Quaglioni and P. Navrátil, Phys. Rev. Lett. **101**, (2008) 092501
19. R. Wiringa, private communication
20. A. Kievsky *et al.*, J. Phys. G: Nucl. Part. Phys. **35**, (2008) 063101
21. M. Viviani, S. Rosati, and A. Kievsky, Phys. Rev. Lett. **81**, (1998) 1580
22. M. Viviani *et al.*, Phys. Rev. Lett. **86**, (2001) 3739
23. R.B. Wiringa, V.G.J. Stoks, and R. Schiavilla, Phys. Rev. C **51**, (1995) 38
24. M.Viviani *et al.*, Few-Body Syst. **39**, (2006) 159
25. L.E. Marcucci *et al.*, Phys. Rev. C **80**, (2009) 034003
26. M.Viviani *et al.*, Few-Body Syst. **45**, (2009) 119
27. D.R. Entem and R. Machleidt, Phys. Rev. C **68**, (2003) 041001
28. E. Epelbaum *et al.*, Phys. Rev. C **66**, (2002) 064001
29. P. Navrátil, Few-Body Syst. **41**, (2007) 117
30. V. Bernard *et al.*, Phys. Rev. C **77**, (2008) 064004
31. B.S. Pudliner *et al.*, Phys. Rev. C **56**, (1997) 1720
32. A. C. Fonseca, Phys. Rev. Lett. **83**, (1999) 4021
33. T. W. Phillips, B. L. Berman, and J. D. Seagrave, Phys. Rev. C **22**, (1980) 384
34. K. F. Famularo *et al.*, Phys. Rev. **93**, (1954) 928
35. D. G. McDonald, W. Haberli, and L. W. Morrow, Phys. Rev. **133**, (1964) B1178
36. B. M. Fisher *et al.*, Phys. Rev. C **74**, (2006) 034001
37. M. T. Alley and L. D. Knutson, Phys. Rev. C **48**, (1993) 1890
38. Y. Koike and J. Haidenbauer, Nucl. Phys. **A463**, (1987) 365c
39. H. Witala, W. Glöckle, and T. Cornelius, Nucl. Phys. **A491**, (1988) 157
40. A. Kievsky *et al.*, Nucl. Phys. **A607**, (1996) 402
41. T.V. Daniels *et al.*, `arXiv:1003.5860`
42. T.V. Daniels, private communication

43. F. Zernike and H.C. Brinkman, Proc. Kon. Ned. Acad. Wensch. **33**, (1935) 3
44. M. Fabre de la Ripelle, Ann. Phys. (N.Y.) **147**, (1983) 281
45. M. Abramowitz and I. Stegun, *Handbook of Mathematical Functions* (Dover Publications, Inc., New York, 1970)
46. M. Viviani, Few-Body Syst. **25**, (1998) 177
47. S. Shimizu *et al.*, Phys. Rev. C **52**, (1995) 1193